UDK 669.14:620.172.2
Original scientific article/Izvirni znanstveni članek

ISSN 1580-2949
MTAEC9, 58(4)503(2024)

INVESTIGATION INTO THE THERMAL DEFORMATION BEHAVIOR AND THE ESTABLISHMENT OF A CONSTITUTIVE RELATIONSHIP FOR Mn-Cr-Ni-Mo STEEL

RAZISKAVA TERMIČNE DEFORMACIJE IN IZDELAVA KONSTITUTIVNEGA MODELA ZA JEKLO VRSTE Mn-Cr-Ni-Mo

Wei Liu[1], Hongchao Ji[1]*, Weimin Yin[2], Yubin Chen[2], Zhiru Dou[2], Xiaoli Yu[2]

[1]College of Mechanical Engineering, North China University of Science and Technology, Tangshan, Hebei, 063210,China.
[2]China MCC22 Group Corporation LTD., Hebei, Tangshan, 063035, China.

Prejem rokopisa – received: 2024-04-06; sprejem za objavo – accepted for publication: 2024-07-02

doi:10.17222/mit.2024.1150

Isothermal compression tests were conducted on Mn-Cr-Ni-Mo steel at temperatures ranging from 1173 K to 1473 K and strain rates from 0.01 s^{-1} to 10 s^{-1} using a Gleeble-3800 thermal simulation tester. Four constitutive models for Mn-Cr-Ni-Mo steel, namely the Arrhenius model, Fields-Backofen model (F-B), original Johnson-Cook model (J-C), and the improved Johnson-Cook model (mJ-C) were established. A correlation coefficient (R) and the average absolute relative error (AARE) were employed to evaluate the predictive capability of these four models. Among them, the Arrhenius model exhibited superior accuracy in predicting the behavior of Mn-Cr-Ni-Mo steel. It and the isothermal thermal compression finite-element model were imported into Deform-3D software for a numerical simulation, aiming to analyze the distribution law of the equivalent stress field. A comparison was made between the time-stress data obtained from numerical simulation under different conditions and that from the isothermal compression tests. The results demonstrate good agreement between the time-stress curves of the numerical simulation and the experimental measurements, indicating that the established Arrhenius model can effectively simulate the thermal deformation of Mn-Cr-Ni-Mo steel. These research findings provide valuable fundamental data for simulating the plastic-deformation process of Mn-Cr-Ni-Mo steel.

Keywords: Mn-Cr-Ni-Mo steel, constitutive model, thermal deformation behavior, finite-element analysis

Avtorji v članku opisujejo visokotemperaturne tlačne preizkuse v temperaturnem območju med 1173 in 1473K in hitrostih deformacije med 0,01 s^{-1} in 10 s^{-1} na jeklu vrste Mn-Cr-Ni-Mo. Preizkuse so avtorji izvajali na termo simulacijskem aparatu Gleeble-3800. Za izdelavo konstitucijskega modela za izbrano jeklo vrste Mn-Cr-Ni-Mo so uporabili oziroma analizirali Arrheniusov model, Fields-Backofen model (F-B), originalni Johnson-Cooksov model (J-C), in izboljšan Johnson-Cook model (mJ-C). Za ovrednotenje sposobnosti napovedi obnašanja vseh štirih izbranih modelov so uporabili korelacijski koeficient (R) in povprečno absolutno relativno napako (AARE; angl.: average absolute relative error). Med izbranimi modeli se je Arrheniusov model za jeklo vrste Mn-Cr-Ni-Mo izkazal z najboljšo sposobnostjo napovedi in najboljšo natančnostjo. Ta model in izotermični tlačni deformacijski model na osnovi končnih elelmentov (FEM; angl.: finite element model) so avtorji vnesli v programsko orodje Deform-3D z namenom analize in porazdelitve zakona obnašanja ekvivalentnega napetostnega polja. Avtorji so primerjali pri različnih pogojih dobljene eksperimentalne podatke *čas-napetost* s podatki dobljenimi z numerično simulacijo. Rezultati analiz so pokazali dobro ujemanje med krivuljami *čas-napetost* numeričnih simulacij z eksperimentalnimi meritvami. Pričujoče raziskave so potrdile, da lahko z Arrheniusovim modelom učinkovito simuliramo termično deformacijo izbranega jekla vrste Mn-Cr-Ni-Mo. Te raziskave po mnenju avtorjev prestavljajo tudi temeljne in kvalitetne podatke za simulacijo procesa plastične deformacije Mn-Cr-Ni-Mo jekel.

Ključne besede: Mn-Cr-Ni-Mo jeklo, konstitutivni model, termična deformacija, analiza s pomočjo metode končnih elementov

1 INTRODUCTION

As one of the most vulnerable components in the ball mill, the ball mill liner is affixed to the inner side of the cylinder to safeguard it against direct impact and grinding from both mill balls and materials.[1–5] The conventional approach for manufacturing ball-mill liners primarily involves casting processes; however, this method is susceptible to defects that can compromise part performance and service life.[6] With the increasing scale and prevalence of ball mills, there are higher demands on the mechanical properties and the longevity of liner parts.[7] Therefore, we propose utilizing a die-forging forming process to enhance the performance of these parts. Typically, high manganese steel, alloy white iron,

and medium-to-low alloy wear-resistant steel are employed as traditional lining materials;[8] however, these materials are mainly suitable for casting processing rather than forging processing. In order to meet both the mechanical properties required for ball-mill liner materials and machinability suitable for forging processing, we have modified the alloying elements and composition based on 40Cr to develop a special Mn-Cr-Ni-Mo steel specifically tailored for forging processes. This type of steel not only fulfills the working requirements for ball-mill liners, but also exhibits excellent mechanical properties and machinability.

The process of thermal deformation is accompanied by the evolution of the microstructure, necessitating an

*Corresponding author's e-mail:
jihongchao@ncst.edu.cn (Hongchao Ji)

Table 1: Chemical composition of test materials (%)

Element	C	Si	Mn	P	S	Cr	Ni	Mo	Fe
Content (*w*/%)	0.432	0.53	1.179	0.0077	0.0035	0.775	0.516	0.179	Balance

investigation into the formation mechanism of hot processing for novel materials. The constitutive model, a mathematical representation reflecting macroscopic material properties, plays a pivotal role in predicting material flow stress and offers a reliable, theoretical foundation for practical production.[9–12] Commonly employed constitutive models encompass the Arrhenius model,[13] Johnson-Cook model,[14] Zerili-Armstrong model,[15] artificial neural network (ANN) approach,[16] Fields-Backofen model,[17] and physics-based constitutive models .[18] Gao et al. developed an Arrhenius constitutive model for a solid-solution-strengthened Ni-Cr-Fe alloy, comprehensively investigating the microstructure evolution and optimizing the hot-working diagram.[13] Ji et al. employed the improved Johnson-Cook constitutive model to characterize the flow-stress equation of a 22MnB5 alloy, in conjunction with the hot-working diagram, and derived the appropriate range for the hot-working process.[14] Gurusamy et al. refined the Zerilli-Armstrong model and established a constitutive model for Inconel718, a nickel-based superalloy. [15]Cai et al. developed an artificial neural network (ANN) model to predict the stress, dynamic recrystallization (DRX) fraction, and DRX grain size of 33Cr23Ni8Mn3N heat-resistant steel.[16] Jia et al. employed the Fields-Backofen constitutive model to characterize the thermal deformation behavior of as-cast AZ31B magnesium alloy and proposed a refined version of the Fields-Backofen constitutive model.[17]

Currently, there is a lack of research on the thermal deformation behavior and constitutive relationship of Mn-Cr-Ni-Mo steel, specifically for the forging process of ball-mill liners. In this study, we conducted an isothermal compression test on Mn-Cr-Ni-Mo steel using the Gleeble-3800 thermal simulation tester. A precise constitutive model was developed to accurately describe the mechanical behavior of Mn-Cr-Ni-Mo steel, thereby establishing a solid foundation for comprehensive prediction of its thermal flow deformation and properties.

2 ISOTHERMAL COMPRESSION EXPERIMENT

2.1 Test materials

The test material is a specially fabricated Mn-Cr-Ni-Mo steel for ball-mill liners, designed to undergo the forging process based on a 40Cr alloy with modified alloying elements and their respective concentrations. Its elemental composition was determined using a direct reading spectrometer and XRD energy spectrum analysis, as presented in **Table 1**. The preparation process is as follows:

The steel is melted to obtain molten steel, followed by the addition of alloying elements for compositional analysis and fine tuning to meet the quality requirements of chemical composition. Subsequently, the molten steel is poured into a 200-mm-diameter mold for casting. After cooling, the resulting billet is heated in a resistance furnace at 1100 °C and maintained at this temperature for 1 h. Then, the forging process is conducted to transform it into a long material with a required section size of 50 mm × 50 mm, as specified by the laboratory. Finally, it is cooled to room temperature.

2.2 Experimental design

The material is extracted from the central region of the cross-section of the prepared Mn-Cr-Ni-Mo steel rod, ensuring that the sample's orientation aligns with that of the rod. The Mn-Cr-Ni-Mo steel was machined into cylindrical specimens with a diameter of 10 mm and a height of 15 mm using an electric spark wire-cutting machine for isothermal compression testing. Subsequently, the cut sample ends were polished to achieve smoothness before conducting the isothermal thermal compression test on a Gleeble-3800 thermal simulation testing machine. The test procedure involved: (1) Applying a layer of graphite sheet at both ends of the sample to minimize friction between the sample and indenter; (2) Heating the sample to the specified temperature at a rate of 100 °C/min using current, followed by holding it for 3 min to ensure complete austenization within the material; (3) Performing isothermal compression tests at dif-

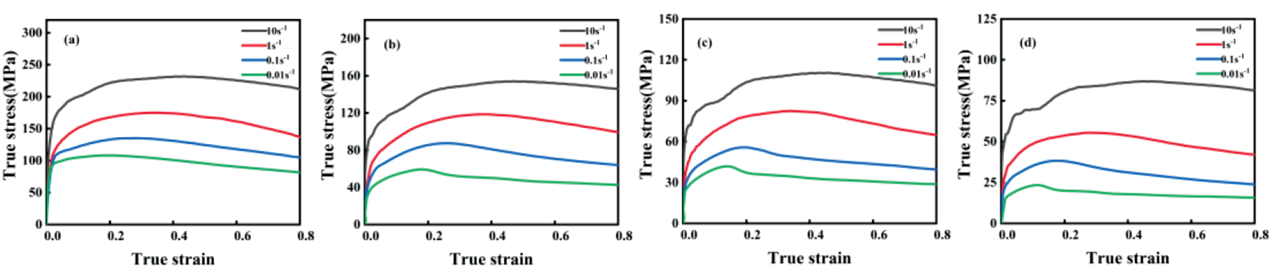

Figure 1: True stress strain curve of Mn-Cr-Ni-Mo steel: a) 1173 K, b) 1273 K, c) 1373 K, d) 1473K

ferent strain rates until reaching a maximum deformation of 60 % for each specimen; and (4) Air-cooling the tested samples to room temperature after completion.

2.3 Experimental result

After analyzing the data obtained from the isothermal hot-compression test using Origin, a data-processing software, we can obtain the high-temperature rheological curve of Mn-Cr-Ni-Mo steel, as depicted in **Figure 1**.

3 CONSTITUTIVE MODEL FOR MN-CR-NI-MO STEEL IS ESTABLISHED

3.1 Arrhenius model and parameter determination based on strain compensation

3.1.1 Reckoning the Arrhenius peak-stress constitutive model

The Arrhenius model is widely employed to elucidate the correlation between strain rate, deformation temperature, and flow stress during high-temperature deformation, effectively capturing the characteristic initial rise followed by a subsequent decline in the stress-strain curve.[19]

$$\dot{\varepsilon}=\begin{cases} A_1\sigma^{m}\exp\left(-\dfrac{Q}{RT}\right) & \alpha\sigma<0.8 \\ A_2\exp(\beta\sigma)\exp\left(-\dfrac{Q}{RT}\right) & \alpha\sigma>1.2 \\ A[\sinh(\alpha\sigma)]^{n}\exp\left(-\dfrac{Q}{RT}\right) & \text{for all } \sigma \end{cases} \quad (1)$$

where R is the molar gas constant, $\dot{\varepsilon}$ is the strain rate, T is the deformation temperature, Q is the activation energy of hot deformation, and A, β, α, m, and n are the material constants.

When the deformation temperature remains constant, combine equation (1) and deform it to obtain:

$$\begin{cases} m=\left[\dfrac{\partial\ln\dot{\varepsilon}}{\partial\ln\sigma}\right]_T \\ \beta=\left[\dfrac{\partial\ln\dot{\varepsilon}}{\partial\ln\sigma}\right]_T \\ n=\left[\dfrac{\partial\ln\dot{\varepsilon}}{\partial\ln(\sinh(\alpha\sigma))}\right]_T \end{cases} \quad (2)$$

The peak stress under different deformation conditions was determined from the stress-strain curve depicted in **Figure 1**. Linear regression analysis using Origin software was performed separately on rows $\ln\dot{\varepsilon}-\ln\sigma_p$ and $\ln\dot{\varepsilon}-\sigma_p$, yielding the results shown in **Figure 2a** and **Figure 2b**, respectively. It can be observed that the slopes of the fitted lines are essentially identical, with an average value of 7.140233. Similarly, fitting the data in **Figure 2b** gives us β as 0.083055 and α as 0.011632 derived from $\alpha=\beta$ /m's values. Likewise, when maintaining a constant strain rate, a fitting line for $\ln\dot{\varepsilon}-\ln[\sinh(\alpha\sigma_p)]$ is plotted (**Figure 2c**). By averaging the slopes of these fitting lines under various deformation conditions, n = 5.0101675 is obtained. Plotting $\ln[\sinh(\alpha\sigma_p)]$ against the reciprocal temperature ($1/T$) and performing linear regression analysis yields a slope

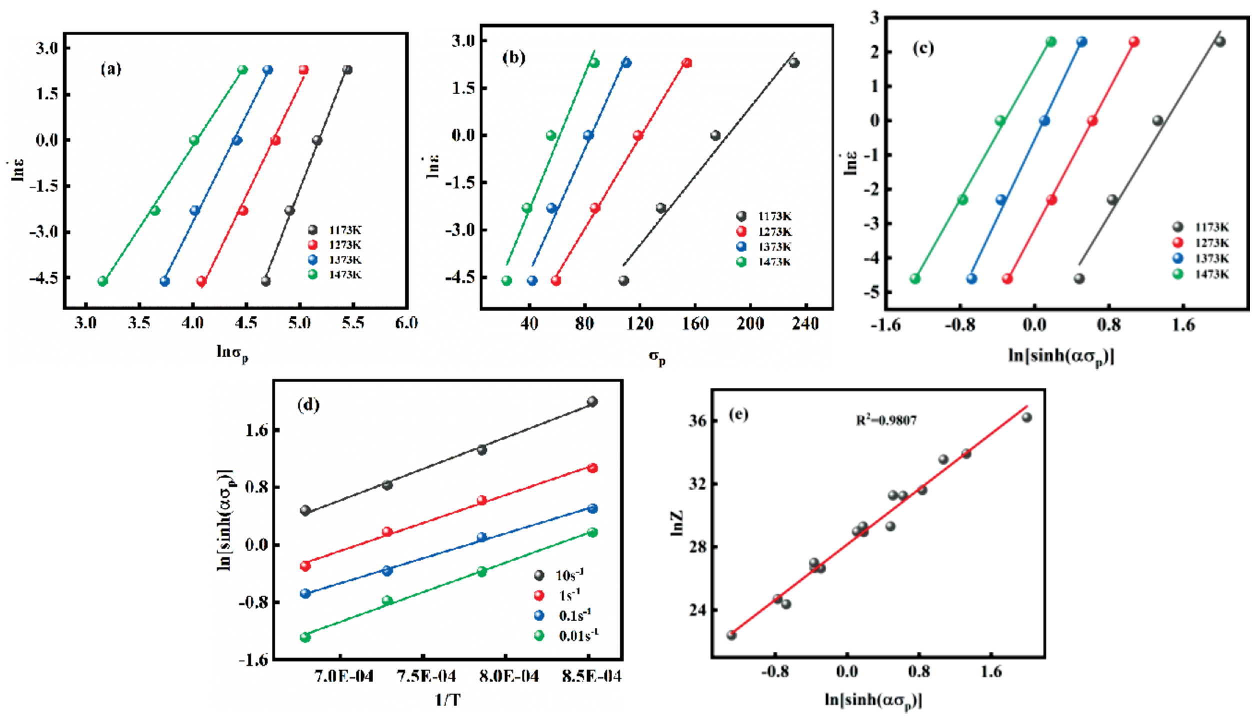

Figure 2: Fitting of relevant parameters: a) $\ln\dot{\varepsilon}-\ln\sigma_p$ linear fitting, b) $\ln\dot{\varepsilon}-\sigma_p$ linear fitting, c) $\ln\dot{\varepsilon}-\ln[\sinh(\alpha\sigma_p)]$ linear fitting, d) $\ln[\sinh(\alpha\sigma_p)]-1/T$ linear fitting, e) $\ln Z-n\ln[\sinh(\alpha\sigma_p)]$ linear fitting

whose average value is $Q/Rn1$ = 7942.156; substituting respective values for R and n gives Q = 330826.8 J/mol as the activation energy for deformation.

The Zener-Hollomon parameter, also referred to as the Z parameter, can be utilized to elucidate the correlation among flow stress, strain rate, and deformation temperature in a scholarly manner.

$$Z = \dot{\varepsilon} \exp\left(\frac{Q}{RT}\right) \tag{3}$$

Combined with equation (1), the above equation and the deformation can be obtained:

$$\ln Z = \ln A + n \ln\left[\sinh(\alpha\sigma)\right] \tag{4}$$

The scatter plots of ln Z and ln $[\sinh(\alpha\sigma_p)]$ are depicted under various deformation conditions, followed by line fitting as illustrated in **Figure 2e**. The intercept of the fitted line corresponds to the value of ln A, with A being equal to $1.71683 \cdot 10^{12}$.

By substituting all the parameters into the equation, the Arrhenius peak stress constitutive model of Mn-Cr-Ni-Mo steel can be derived as follows:

$$\begin{cases} \dot{\varepsilon} = 1.71683\times10^{12}\left[\sinh(0.011632\sigma_p)\right]^{5.0101675}\exp\left(-\dfrac{330826.8}{8.31T}\right) \\ Z = \dot{\varepsilon}\cdot\exp\left(-\dfrac{330826.8}{RT}\right) \\ \sigma_p = \dfrac{1}{0.011632}\ln\left\{\left(\dfrac{Z}{1.71683\times10^{12}}\right)^{\frac{1}{5.0101675}} + \left[\left(\dfrac{Z}{1.71683\times10^{12}}\right)^{\frac{2}{5.0101675}}+1\right]^{\frac{1}{2}}\right\} \end{cases} \tag{5}$$

3.1.2 Reckoning the Arrhenius model based on strain compensation

The constitutive model of peak stress can solely predict the maximum deformation resistance of the material, without being able to anticipate the variation in flow stress throughout the entire deformation process. To enhance the predictive accuracy of the Mn-Cr-Ni-Mo steel's constitutive model, strain is incorporated into the prediction model, resulting in a comprehensive constitutive model that accounts for strain. In this study, several strain variables are selected within a range 0.05–0.8 with an interval of 0.05. A flow-stress prediction model is established for each strain, and the material parameters obtained in each model are fitted. The accuracy of fitting is found to be the highest when using a seventh-degree polynomial. The relationship between material parameters and dependent variables can be accurately represented by a seventh-degree polynomial through fitting the experimental results. Consequently, this polynomial enables the calculation of material parameters for any given set of dependent variables. Subsequently, by plugging in each deformation condition into equation (3), the Z parameter can be calculated for each condition. Finally, by substituting the obtained material parameters and corresponding Z parameters into equation (4) for a true stress calculation, the corresponding true stress value of Mn-Cr-Ni-Mo steel under any strain variable can be determined.

3.1.3 Verification of the Arrhenius model with strain compensation

The equation of the Arrhenius model with strain compensation for Mn-Cr-Ni-Mo steel is presented below, and the corresponding prediction results are illustrated in **Figure 3**.

$$\begin{aligned} a &= 0.01435 + 0.00686\varepsilon - 0.3275\varepsilon^2 + 2.24316\varepsilon^3 - \\ &+7.00132\varepsilon^4 + 11.43629\varepsilon^5 - 9.47502\varepsilon^6 + 3.14204\varepsilon^7 \\ n &= 3.56216 + 72.75132\varepsilon - 762.687\varepsilon^2 + 3518.929\varepsilon^3 - \\ &-8781\varepsilon^4 + 12276.28\varepsilon^5 - 9040.35\varepsilon^6 + 2729.62\varepsilon^7 \\ Q &= 296555 + 830762\varepsilon - 7438410\varepsilon^2 + 3.25\times10^7\varepsilon^3 - \\ &78195700\varepsilon^4 + 1.06\times10^8\varepsilon^5 - 76182000\varepsilon^6 + 2.26\times10^7\varepsilon^7 \\ \ln A &= 26.65684 + 38.39359\varepsilon - 356.838\varepsilon^2 + 1530.47\varepsilon^3 - \\ &-3481.45\varepsilon^4 + 4388.434\varepsilon^5 - 2908.96\varepsilon^6 + 792.1565\varepsilon^7 \\ \sigma &= \left(\frac{1}{\alpha}\right)\ln\left\{\left(\frac{Z}{A}\right)^{1/n} + \left[\left(\frac{Z}{A}\right)^{2/n}+1\right]^{1/2}\right\} \\ Z &= \dot{\varepsilon}\cdot\exp\left(\frac{Q}{RT}\right) \end{aligned} \tag{6}$$

3.2 Parameter determination of F-B model, J-C model and mJ-C model

Additionally, we have also established the F-B model, J-C model and mJ-C model for Mn-Cr-Ni-Mo steel and determined the corresponding parameters. The

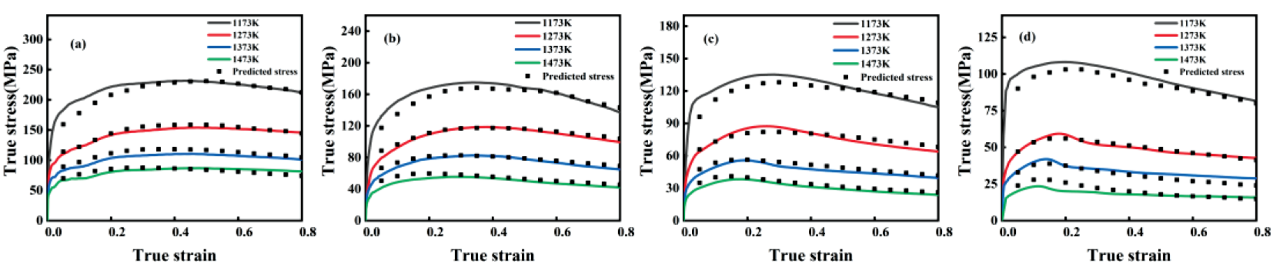

Figure 3: Comparison of Arrhenius model with strain compensation predicted values with experimental values: a) $\dot{\varepsilon}$ = 10 s^{-1}; b) $\dot{\varepsilon}$= 1 s^{-1}; c) $\dot{\varepsilon}$ = 0.1 s^{-1}; d) $\dot{\varepsilon}$ = 0.01 s^{-1}

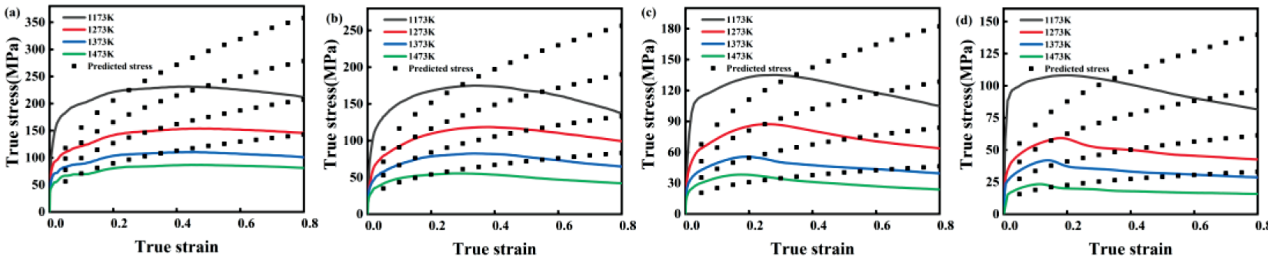

Figure 4 Comparison of F-B model predicted values with experimental values: a) $\dot{\varepsilon}$ = 10 s^{-1}, b) $\dot{\varepsilon}$ = 1 s^{-1}, c) $\dot{\varepsilon}$ = 0.1 s^{-1}, d) $\dot{\varepsilon}$ = 0.01 s^{-1}

constitutive models are presented below, while the prediction results are illustrated in **Figure 4**, **Figure** 5 and **Figure 6**.

F-B:
$$\sigma = \left(-651.54 + 20.014\log\dot{\varepsilon} + \frac{1091321}{T}\right)\cdot \varepsilon^{0.0061+0.0218\log\varepsilon+\frac{373.134}{T}} \cdot \dot{\varepsilon}^{0.0001002T+0.000147} \quad (7)$$

J-C:
$$\begin{cases} \sigma = (75.31 + 5.609061\varepsilon^{-0.4021})(1+0.18052\ln\dot{\varepsilon}^{*})(1-T^{*0.63}) \\ \dot{\varepsilon}^{*} = \dot{\varepsilon}/\dot{\varepsilon}_0 \\ T^{*} = (T-T_{\mathrm{r}})/(T_{\mathrm{m}}-T_{\mathrm{r}}) \end{cases} \quad (8)$$

mJ-C:
$$\begin{aligned} \sigma = {} & (96.87675 + 108.8253\varepsilon - 327.447\varepsilon^2 + \\ & +211.4949\varepsilon^3)(1+0.18402\ln\dot{\varepsilon}^{*})\cdot \\ & \cdot\exp\left[(-0.00537+0.000305\ln\dot{\varepsilon}^{*})(T-T_{\mathrm{r}})\right] \end{aligned} \quad (9)$$

4 ACCURACY EVALUATION OF THE CONSTITUTIVE MODEL OF Mn-Cr-Ni-Mo STEEL

To provide a more precise explanation of the predictive accuracy of the equation, correlation coefficient (R) and average absolute relative error (AARE) were employed to evaluate the predictive capability of these four models. The following equation is employed:

$$R = \frac{\sum_{i=1}^{N}(\sigma_{Ei}-\bar{\sigma}_{E})(\sigma_{Pi}-\bar{\sigma}_{Pi})}{\sqrt{\sum_{i=1}^{N}(\sigma_{Ei}-\bar{\sigma}_{E})^2\sum_{i=1}^{N}(\sigma_{Pi}-\bar{\sigma}_{Pi})^2}} \quad (10)$$

$$AARE(\%) = \frac{1}{N}\sum_{i=1}^{N}\left|\frac{\sigma_{Ei}-\sigma_{Pi}}{\sigma_{Ei}}\right| \quad (11)$$

where, σ_{Ei} and $\bar{\sigma}_{\mathrm{E}}$ represent the test value and the average value of the test value respectively, MPa; σ_{Pi} and $\bar{\sigma}_{\mathrm{Pi}}$ represent the predicted value and the average value of the predicted value respectively, MPa; N indicates the total number of data.

A smaller AARE (%) value indicates a closer proximity between the two sets of data, while a larger R value signifies a stronger correlation. The AARE values and R values of the four constitutive models are presented in **Table 2**. From the results depicted in the table, it is evident that the Arrhenius model exhibits robust predictive capabilities, whereas the F-B model demonstrates relatively limited forecasting abilities.

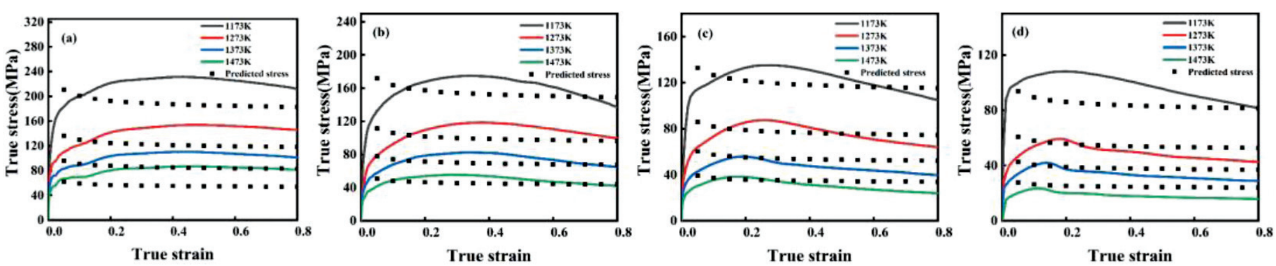

Figure 5: Comparison of J-C model predicted values with experimental values: a) $\dot{\varepsilon}$ = 10 s^{-1}, b) $\dot{\varepsilon}$ = 1 s^{-1}, c) $\dot{\varepsilon}$ = 0.1 s^{-1}, d) $\dot{\varepsilon}$ = 0.01 s^{-1}

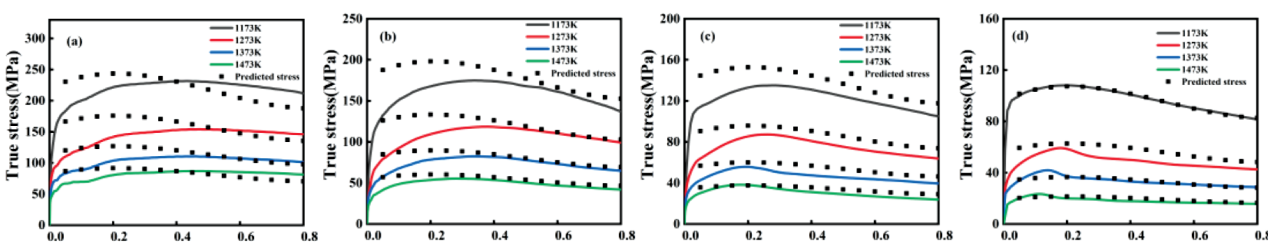

Figure 6: Comparison of mJ-C model predicted values with experimental values: a) $\dot{\varepsilon}$ = 10 s^{-1}, b) $\dot{\varepsilon}$ = 1 s^{-1}, c) $\dot{\varepsilon}$ = 0.1 s^{-1}, d) $\dot{\varepsilon}$ = 0.01 s^{-1}

Table 2: AARE and R of four constitutive models

Item	Arrhenius	F-B	J-C	m J-C
AARE (%)	7.1286	22.2	12.1	10.4
R	0.985803	0.883	0.965234	0.975347

The established strain compensation Arrhenius model of Mn-Cr-Ni-Mo steel yields predicted values that closely match the experimental measurements, indicating a relatively high prediction accuracy for the proposed model equation in this study. The AARE and R values were further improved to 7.13 % and 0.986, respectively. The calculated values of the F-B model for Mn-Cr-Ni-Mo steel exhibit excellent agreement with the experimental data prior to reaching peak stress. As depicted in **Figure 4**, this model solely captures the strain-hardening stage of Mn-Cr-Ni-Mo steel. However, experimental results reveal a recrystallization softening phenomenon during thermal deformation, which cannot be accurately described by the F-B model. The AARE and R values were 22.2 % and 0.883, respectively. The J-C model for Mn-Cr-Ni-Mo steel offers the advantage of requiring fewer parameters, being easily obtainable from limited experiments, and simple to implement. However, it also has several limitations. The described thermal softening behavior exhibits a rough linearity but deviates to some extent from the actual test measurements due to assuming strain hardening, strain-rate strengthening, and thermal softening as independent phenomena that can be separated from each other. This assumption overlooks the coupling effect of strain, strain rate, and temperature on a material's rheological behavior. The values of AARE and R were determined to be 12.1 % and 0.965 respectively. The mJ-C model for Mn-Cr-Ni-Mo steel incorporates the coupling relationship between temperature and strain rate, thereby addressing certain limitations of its original counterpart, while maintaining better predictive capabilities. The AARE and R values are 10.4 % and 0.975, respectively.

The correlation between the four constitutive models and the test results is illustrated in **Figure 7**. The accuracy of the model's prediction relies on the proximity of data points to the solid line, with a higher concentration indicating a stronger correlation between the model and test values. It can be observed that the Arrhenius model effectively characterizes the hot-deformation behavior of Mn-Cr-Ni-Mo steel.

5 CONSTITUTIVE MODEL VERIFICATION OF Mn-Cr-Ni-Mo STEEL

The thermal deformation behavior of Mn-Cr-Ni-Mo steel was investigated at various deformation temperatures and strain rates using Deform-3D finite-element software. A well-fitting constitutive model was employed to numerically simulate the isothermal thermal shrinkage test under different conditions. Based on the precision comparison presented in Table 2, the Arrhenius model exhibited strong correlation with experimental data obtained at different strain rates. By utilizing ABSOFT and FORTRAN programming languages, the finite-element user sub-routine was compiled to establish an EXE file, which enabled the input of the model into the finite-element software. Subsequently, a comparison between the time-stress curve obtained from Deform-3D

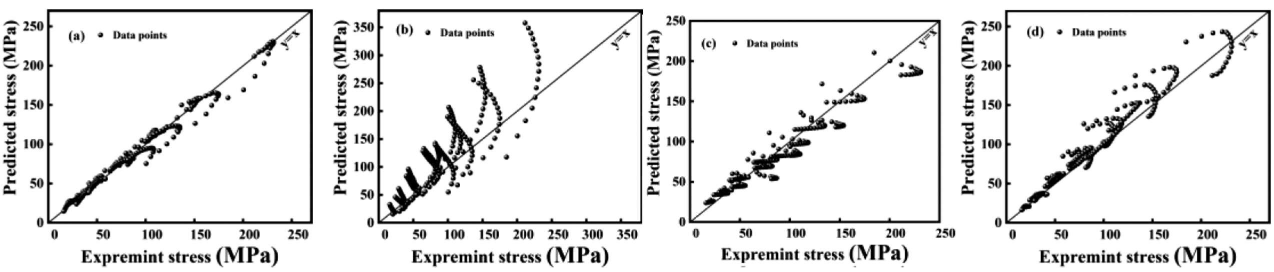

Figure 7: Correlation between constitutive model and test results; a) Arrhenius; b) F-B; c) J-C ; d) mJ-C

Table 3: Hot-forging process parameters of ball-mill liner

Argument	Value
Top die speed (mm/s)	$V_{10} = -10\ x + 150$, $V_1 = -x + 15$ $V_{0.1} = -0.1\ x + 1.5$, $V_{0.01} = -0.01\ x + 0.15$ (x is the travel)
Initial temperature of test element (K)	1173, 1273, 1373, 1473
Initial die temperature (K)	1173, 1273, 1373, 1473
Ambient temperature (K)	1173, 1273, 1373, 1473
Heat-transfer coefficient (N/s/mm/K)	1
Convection coefficient (N/s/mm/K)	0.02
Friction coefficient	0.3
Number of blank grids	150000
Die material	AISIH13
Test-piece material	Mn-Cr-Ni-Mo steel

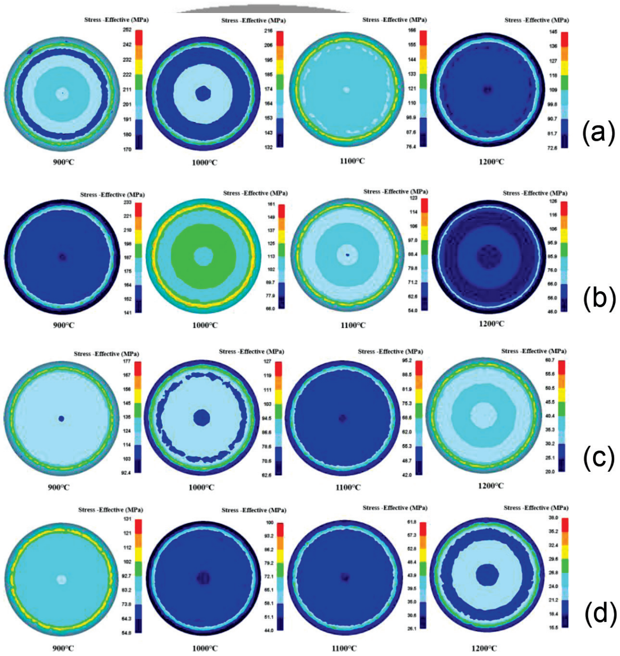

Figure 9: Equivalent stress cloud diagram of the isothermal thermal compression test piece of Mn-Cr-Ni-Mo steel: a) $\dot{\varepsilon}$ = 10 s^{-1}, b) $\dot{\varepsilon}$ = 1 s^{-1}, c) $\dot{\varepsilon}$ = 0.1 s^{-1}, d) $\dot{\varepsilon}$ = 0.01 s^{-1}

numerical simulation for isothermal thermal compression test and that acquired through experimental means was conducted to validate the accuracy of the simulation.

5.1 Establishment of finite-element model

The three-dimensional geometric models of both the isothermal compression standard test specimen and simplified isothermal compression testing apparatus were created using Solidworks software. Afterwards, these models were imported into Deform-3D software as STL files for pre-processing to establish a numerical simulation finite-element model for conducting isothermal thermal compression tests. The process of constructing this model mainly consisted of five steps: grid division, material assignment, defining boundary conditions, positioning the models accurately within it and configuring relevant process parameters accordingly (as shown in **Table 3**). **Figure 8** depicts a simplified three-dimensional thermal coupling model used in performing such tests with Deform-3D.

5.2 Analysis of simulation results

According to the numerical simulation results, the isothermal thermal compression test piece of Mn-Cr-Ni-Mo steel yielded an equivalent stress cloud diagram, as depicted in **Figure 9**. It can be observed that the distribution of equivalent stress in the test piece is relatively homogeneous, with most areas exhibiting a difference in equivalent stress values within 20MPa. The gradual increase in equivalent stress distribution from the center to the edge position indicates more intense metal flow at the edge during hot compression compared to that at the center. The stress distribution in the larger area is consistent with the equivalent stress at the end of the flow-stress curve, thereby affirming the accuracy of our numerical simulation.

In order to visually demonstrate the accuracy of numerical simulation in describing isothermal hot compression tests, four distinctive points were carefully selected from Mn-Cr-Ni-Mo steel specimens for comprehensive investigation. The feature points are evenly distributed from the center to the edge of the test piece. The average equivalent stress value of the four feature points was determined throughout the simulation process. A time-equivalent stress curve was plotted and compared with data obtained from isothermal thermal compression tests, as depicted in **Figure 10**. It can be observed that the Arrhenius model accurately assessed both the material's response characteristics in thermal deformation behavior and exhibited good agreement with the experimental values. These results affirm the correctness of the Arrhenius model for simulating Mn-Cr-Ni-Mo steel's thermal deformation.

6 CONCLUSIONS

In this study, the isothermal compression test of Mn-Cr-Ni-Mo steel for a ball-mill liner suitable for a forging process was conducted using a Gleeble-3800 thermal simulation testing machine at various temperatures and strain rates. Four constitutive models were established, including Arrhenius model, F-B model, J-C model and mJ-C model. Deform-3D finite-element software was utilized to simulate equivalent thermal compression tests. The specific results are as follows:

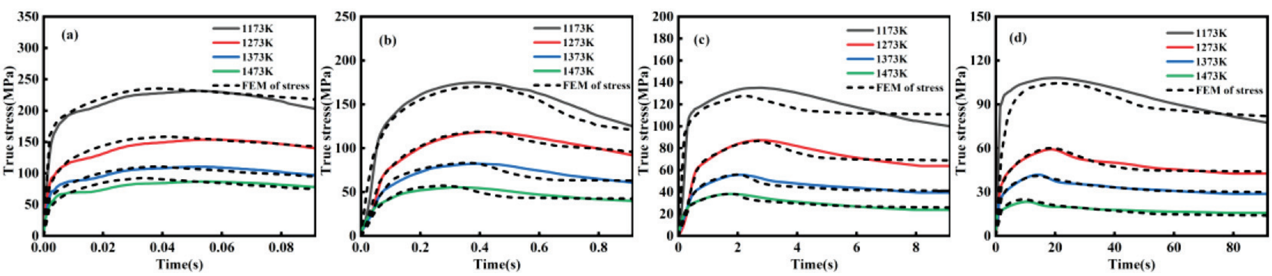

Figure 10: Comparison of time-equivalent stress curves between test and numerical simulation: a) $\dot{\varepsilon}$ = 10 s^{-1}, b) $\dot{\varepsilon}$ = 1 s^{-1}, c) $\dot{\varepsilon}$ = 0.1 s^{-1}, d) $\dot{\varepsilon}$ = 0.01 s^{-1}

(1) The predictive ability of four constitutive models was evaluated using the correlation coefficient (R) and average absolute relative error (AARE). Among them, the Arrhenius model for Mn-Cr-Ni-Mo steel demonstrated the highest level of prediction accuracy, AARE (%) and R are 7.13% and 0.986, respectively. The F-B model exhibited the lowest level of prediction accuracy, AARE (%) and R are 22.2 % and 0.883, respectively. The J-C model ranked third in terms of prediction accuracy, followed by the mJ-C model, which ranked second. A smaller AARE (%) value indicates a closer proximity between the two sets of data, while a larger R value signifies a stronger correlation.

(2) The Arrhenius model and isothermal thermal compression finite-element model were incorporated into the Deform-3D software for a numerical simulation. The results demonstrated a strong agreement between the time-stress curves obtained from both numerical simulation and experimental data, validating the applicability of the established Arrhenius model in simulating the thermal deformation of Mn-Cr-Ni-Mo steel.

Acknowledgement

This research was financially supported by the Science and Technology Project of China Minmetals Corporation Limited (2021ZXA06).

7 REFERENCES

[1] L. Anggraini, et al.: Predictive maintenance on ball mill liner using 3D scanner and its analysis in the mining industry of Papua Indonesia. Results in Engineering, 20 (**2023**), doi:10.1016/j.rineng.2023.101568

[2] L. Xu, S. Bao, Y. Zhao: Multi-level DEM study on liner wear in tumbling mills for an engineering level approach. Powder Technology, 364 (**2020**) 332–342, doi:10.1016/j.powtec.2020.02.004

[3] Y. X. Peng et al.: Experimental Study on Multibody Friction and Wear Properties of Liner in Ball Mills. Tribology Transactions, 64 (**2021**) 253–263, doi:10.1080/10402004.2020.1831120

[4] C. T. Jayasundara, H. Zhu: Predicting liner wear of ball mills using discrete element method and artificial neural network. Chemical Engineering Research & Design, 182 (**2022**) 438–447, doi:10.1016/j.cherd.2022.04.013

[5] N. Chimwani, M. M. Bwalya: Exploring the End-Liner Forces Using DEM Software. Minerals, 12 (**2020**), doi:10.3390/min10121047

[6] C. Chelladurai, et al.: Analyzing the casting defects in small scale casting industry. in International Conference on Newer Trends and Innovations in Mechanical Engineering (ICONTIME) - Materials Science. (2020) Electr Network, doi:10.1016/j.matpr.2020.05.382

[7] W. W. Liu, et al.: Study on impact dynamic characteristics of semi-autogenous mill liner based on improved multivariable method. Heliyon, 11 (**2022**), doi:10.1016/j.heliyon.2022.e11526

[8] Y. Liu, Study on liquid die forging of ball mill liner material and its microstructure properties. 2017

[9] D. G. He, et al.: Microstructure evolution and constitutive model for a Ni-Mo-Cr base alloy in double-stages hot compression with step-strain rates. Materials Characterization, 194 (**2022**), doi:10.1016/j.matchar.2022.112385

[10] Y. C. Lin, et al.: Constitutive models for high-temperature flow behaviors of a Ni-based superalloy. Materials & Design, 59 (**2014**) 115–123, doi:10.1016/j.matdes.2014.02.041

[11] H. C. Ji, et al.: Optimization the working parameters of as-forged 42CrMo steel by constitutive equation-dynamic recrystallization equation and processing maps. Journal of Materials Research and Technology-Jmr&T, 4 (**2020**) 7210–7224. doi:10.1016/j.jmrt.2020.04.078

[12] P. F. Gao, et al.: Deformation behavior and microstructure evolution of titanium alloys with lamellar microstructure in hot working process: A review. Journal of Materials Science & Technology, 39 (**2020**) 56–73. doi:10.1016/j.jmst.2019.07.052

[13] S. Gao, et al.: Hot deformation behavior and hot working window of a solid solution strengthened Ni–Cr–Fe-based superalloy. Journal of Materials Research and Technology, 29 (**2024**) 1377–1389. doi:https://doi.org/10.1016/j.jmrt.2024.01.149

[14] H. C. Ji, et al.: HOT-DEFORMATION BEHAVIOR AND PROCESSING MAP OF 22MnB5 HIGH-STRENGTH STEEL. Materiali in Tehnologije, 57 (**2023**) 367–378. doi:10.17222/mit.2023.874

[15] M. M. Gurusamy, B. C. Rao: On the performance of modified Zerilli-Armstrong constitutive model in simulating the metal-cutting process. Journal of Manufacturing Processes, 28 (**2017**) 253–265. doi:10.1016/j.jmapro.2017.06.011

[16] Z. M. Cai, et al.: An Investigation into the Dynamic Recrystallization (DRX) Behavior and Processing Map of 33Cr23Ni8Mn3N Based on an Artificial Neural Network (ANN). Materials, 13 (2020), doi:10.3390/ma13061282

[17] W. T. Jia, et al.: Modified Fields-Backofen model for constitutive behavior of as-cast AZ31B magnesium alloy during hot deformation. Materials & Design, 106 (**2016**) 120–132. doi:10.1016/j.matdes.2016.05.089

[18] Y. M. Huo, et al.: Microstructure evolution and unified constitutive equations for the elevated temperature deformation of SAE 52100 bearing steel. Journal of Manufacturing Processes, 44 (**2019**) 113–124. doi:10.1016/j.jmapro.2019.05.051

[19] J. Jonas, C. Sellars, W. M. Tegart: Strength and structure under hot-working conditions. Metallurgical reviews, 14 (**1969**) 1–24